Differentiating Geometric Isomers by Laser–Ion Beam Photodissociation

R. E. Krailler and D. H. Russell*

Department of Chemistry, Texas A&M University, College Station, Texas 77843

The laser–ion beam photodissociation reactions of the *cis*-1,3-pentadiene and *trans*-1,3-pentadiene $C_5H_8^+$ ions and the *cis*,*trans*-2,4-hexadiene and *trans*,*trans*-2,4-hexadiene $C_6H_{10}^+$ ions have been investigated. The photodissociation spectra are found to agree qualitatively with the published ion cyclotron resonance (ICR) photodissociation data. Although the $C_5H_8^+$ and $C_6H_{10}^+$ geometric isomers exhibit indistinguishable photodissociation spectra and product ion branching ratios, the wavelength-dependent kinetic energy release values are unique for the individual isomers. The significant changes in the photofragment kinetic energy release values for the *trans*-1,3-pentadiene and *trans*,*trans*-2,4-hexadiene ions as a function of photon energy are attributed to isomerization of the photoexcited parent ion prior to dissociation.

Differentiation of structural isomers by mass spectrometry has been aided by the development of new methods such as collision-induced dissociation (CID), photoelectron photoion coincidence, ion–molecule reaction chemistry, and laser–ion beam photodissociation. One class of isomers, however, has remained difficult to differentiate, viz., geometric isomers and stereoisomers. Ion cyclotron resonance photodissociation (ICR-PDS) studies have had some success in distinguishing cis/trans isomers. For example, Dunbar et al. have successfully differentiated the isomeric *cis*- and *trans*-chloropropene ions (*1*, *2*) and the *trans,trans*-, *cis,trans*-, and *cis,cis*-2,4-hexadiene radical cations (*3*). In contrast, Dunbar has found no detectable differences in the ICR-PDS data for the *cis*- and *trans*-1,3,5-hexatriene ions (*4*) or for the *cis*- and *trans*-2-butene ions (*5*). In addition, van der Hart was not able to distinguish between *cis*- and *trans*-1,3-butadienenitriles (*6*) and could only provide indirect measurements for the isomerization of *cis*- and *trans*-2-pentenes (*7*). Finally, Brauman et al. could not differentiate the *cis*- and *trans*-stilbene isomers using ICR-PDS (*8*).

In general the lack of definative data for isomeric systems is interpreted as complete or partial isomerization of the geometric isomers to the more stable ion form. It is, however, difficult to rule out the possibility that the ICR-PDS measurements may be insensitive to the subtle structural differences of the geometric forms.

We initiated the laser–ion beam photodissociation studies of the geometric isomers of *cis*- and *trans*-1,3-pentadiene and *cis,trans*- and *trans,trans*-2,4-hexadiene to answer two specific questions. First, would laser–ion beam photodissociation, which is thought to sample ions having a wider range of internal energies than ICR-PDS (*9*), be able to differentiate between known noninterconverting structures? Second, if the technique were successful, would it be of general utility? Earlier laser–ion beam photodissociation work by Beynon suggests that measurements of the kinetic energy released on photodissociation may be used as a structural probe (*10–13*). In particular, Beynon has shown that the relationship between energy partitioning (kinetic energy release) and total energy of the dissociationing ion (wavelength of the photon) may provide dynamical information about the dissociation reaction as well as structural information.

EXPERIMENTAL SECTION

The experimental apparatus used for these studies is shown schematically in Figure 1. The apparatus consists of a Kratos (A.E.I.) MS-902S double focusing mass spectrometer, a Coherent CR-18 argon ion laser, and necessary electronic components for laser modulation and signal detection. The mass spectrometer is equipped with a programmable high-voltage power supply (Wallis, Model R103/3), a digital wave form generator (Wavetek, Model 159) for programming the high-voltage supply, and an adjustable energy resolving slit (β slit). The accelerating potential is monitored by a Keithley $4^1/_2$ digit multimeter. The laser beam is aligned coaxially with the ion beam using mirrors with micrometer adjustments for fine control. The laser is focused to a spot size of ca. 0.1 mm by using a 500 mm focal length convex lens. In this mode, the focal point of the laser beam coincides with the beam-defining slit (source slit) which gives maximum overlap of the laser and ion beams. Laser–ion beam alignment is accomplished by adjusting the mirrors to achieve a maximum photodissociation signal (at 488 nm) for loss of H from $C_6H_6^+$ ions formed by direct ionization of 2,4-hexadiyne. The laser beam enters the ion source housing through a sapphire window mounted on the source flange, passes through the ion source repellar (aperature 1 mm diameter), and enters the first field-free region. In addition, perpendicular laser–ion beam experiments can be performed by admitting the laser beam into the first field-free region through a sapphire window mounted onto the analyzer housing. For maximum sensitivity the majority of the experiments were performed using a coaxial laser–ion beam configuration; however, critical data were remeasured by using a perpendicular laser–ion beam configuration. No significant differences between the two configurations were observed.

Photofragment ions formed in the first field-free region are transmitted through the electrostatic analyzer by scanning the accelerating voltage over a small range centered about $V(m_2/m_1)$ (where m_1 and m_2 are the masses of the parent ion and fragment ion, respectively, and V is the accelerating voltage required to focus the main beam). Unimolecular metastable ion and residual collision-induced dissociation (CID) occurring in the first field-free region yields a signal more than 10 times larger than the photofragment ion signal. The photofragment ion signal is detected by mechanically chopping the laser beam and measuring the difference between the laser "on" and "off" signals. The difference signal is obtained by using a lock-in amplifier (PAR, Model 124A). To enhance the signal-to-noise ratio, the signal is accumulated and averaged with a Nicolet 1174 signal averager. The high-voltage scanning and signal averaging are slaved to the wave form generator.

Discrimination against product ions with a large velocity component perpendicular to the ion beam direction is a problem with the instrumental configurations employed in this experiment. However, for the data reported here no significant errors are expected because the product ion relative kinetic energies are small.

The experiments were performed under low-pressure electron impact ionization conditions. In all cases the ionizing conditions were 70 eV electron energy and emission currents of 500 μA. The effect of different ionizing energies (15–70 eV) was examined and no detectable differences were found. All reagents were obtained from commercial sources: *cis*-1,3-pentadiene (Chemical Procurement Laboratories), *trans*-1,3-pentadiene, and *cis,trans*- and *trans,trans*-2,4-hexadiene (Pfaltz and Bauer). The samples were purified by several freeze–pump–thaw cycles to remove any noncondensable gases.

0003-2700/85/0357-1211$01.50/0

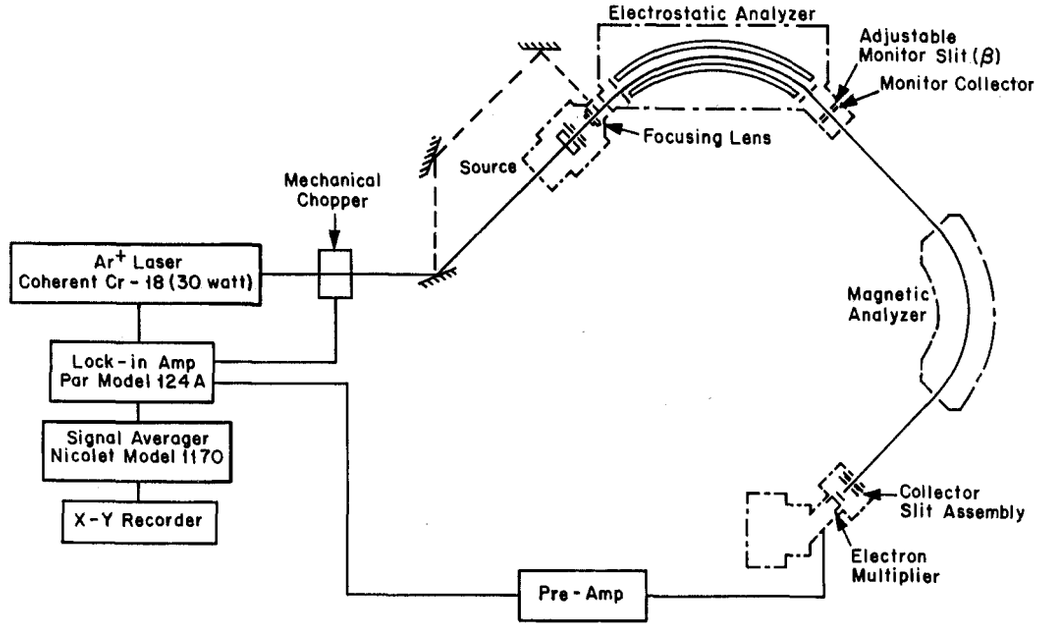

Figure 1. *Schematic diagram of the laser–ion beam photodissociation apparatus.*

Table I. Wavelength-Dependent Branching Ratios for *cis*- and *trans*-1,3-Pentadiene, $C_5H_8^+$

	cis-1,3-pentadiene						*trans*-1,3-pentadiene					
	514 nm	502 nm	496 nm	488 nm	476 nm	458 nm	514 nm	502 nm	496 nm	488 nm	476 nm	458 nm
$C_5H_7^+$	91.1	89.0	87.6	85.9	87.3	77.3	93.1	89.6	89.4	88.9	91.7	67.6
$C_5H_6^+$	7.8	8.5	9.9	10.7	9.1	17.0	1.4	2.2	2.3	4.0	1.6	4.4
$C_4H_5^+$	1.2	1.1	1.5	1.9	2.1	3.8	4.8	6.8	6.8	5.9	5.3	22.7
$C_3H_6^+$	0.5	0.6	0.5	0.5	0.4	0.5	0.5	0.7	0.8	0.8	0.7	2.7
$C_3H_4^+$	0.5	0.5	0.2	0.9	0.9	1.7	0.7	0.8	0.9	0.6	0.5	2.4

Table II. Wavelength-Dependent Branching Ratios of *cis,trans*- and *trans,trans*-2,4-Hexadiene, $C_6H_{10}^+$

	cis,trans-2,4-hexadiene						*trans,trans*-2,4-hexadiene					
	514 nm	502 nm	496 nm	488 nm	476 nm	458 nm	514 nm	502 nm	496 nm	488 nm	476 nm	458 nm
$C_6H_9^+$	13.8	15.0	16.1	15.5	13.9	15.4	8.2	6.9	8.0	7.6	7.4	7.7
$C_5H_7^+$	82.1	80.5	79.8	79.6	82.0	80.4	88.8	91.1	88.9	89.4	90.2	90.3
$C_4H_6^+$	5.6	5.8	5.4	6.2	5.7	5.4	3.2	2.8	3.5	3.4	3.1	3.2

RESULTS

As part of this work we have investigated the visible wavelength photodissociation of the molecular ions of two pairs of geometric isomers, viz., *cis*- and *trans*-1,3-pentadiene ($C_5H_8^+$) and *cis,trans*- and *trans,trans*-2,4-hexadiene ($C_6H_{10}^+$). All four compounds produce molecular ions which undergo photodissociation in the visible wavelength range of the argon ion laser (514.5–458 nm).

The photodissociation reactions observed for the $C_5H_8^+$ and $C_6H_{10}^+$ ions are shown in reactions 1–8.

$$C_5H_8^+ \xrightarrow{h\nu} \begin{cases} C_5H_7^+ + H & (1) \\ C_5H_6^+ + H_2 & (2) \\ C_4H_5^+ + CH_3 & (3) \\ C_3H_6^+ + C_2H_2 & (4) \\ C_3H_4^+ + C_2H_4 & (5) \end{cases}$$

$$C_6H_{10}^+ \xrightarrow{h\nu} \begin{cases} C_6H_9^+ + H & (6) \\ C_5H_7^+ + CH_3 & (7) \\ C_4H_6^+ + C_2H_4^+ & (8) \end{cases}$$

Studies on the laser power dependence for the photofragment signals are consistent with the observed photodissociation arising from a single photon process. Also, the thermochemical data for these systems are consistent with the photofragment ions having appearance energies in the range of 2.1–2.7 eV (*14*).

The photofragment ion spectra are obtained by summing the photodissociation product ion abundances at a given wavelength and correcting for the change in the photon flux. The photofragment ion spectra for the two $C_5H_8^+$ ions are shown in Figure 2. The spectra are bimodal with maxima at 502 and 476 nm and are indistinguishable. The spectra for the $C_6H_{10}^+$ isomers are shown in Figure 3. These spectra are also bimodal with a maximum at 502 nm and a broad diffuse band at ca. 465 nm. These spectra are also indistinguishable.

The branching ratios for the product ions from the *cis*-$C_5H_8^+$ ions are given in Table I. The branching ratio data for the *cis,trans*- and *trans,trans*-$C_6H_{10}^+$ ions are given in Table II. The branching ratios were derived from photofragment ion abundances using integrated peak areas. In this experiment the photofragment ions are detected by accelerating voltage scanning. The precursor ions are transmitted through the electrostatic analyzer (ESA) with a nominal energy of 4 keV, and to focus a particular fragment ion requires scanning the high voltage over a narrow energy range centered about $V(m_1/m_2)$ (see Experimental Section). As different product ions (m_2) are monitored, the time required for the m_1 ions to traverse the first field-free region will decrease by $(m_1/m_2)^{-1/2}$. To account for the change in the resident time

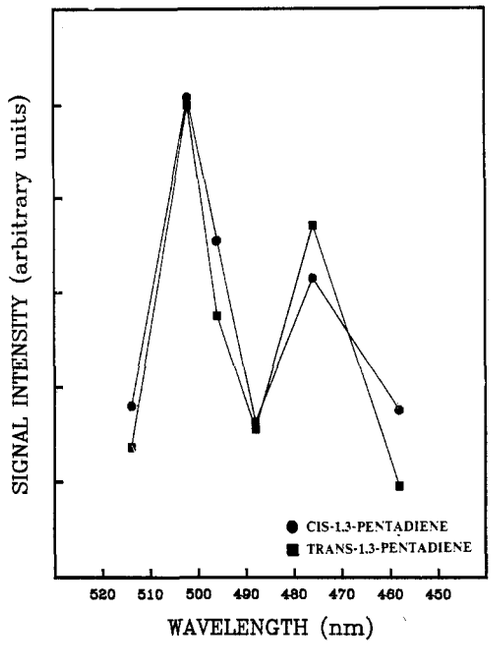

Figure 2. Photofragment ion spectra for *cis*-1,3-pentadiene (●) and *trans*-1,3-pentadiene (■). The line joining the data points is a guide to give an indication of the shape of the absorption profile.

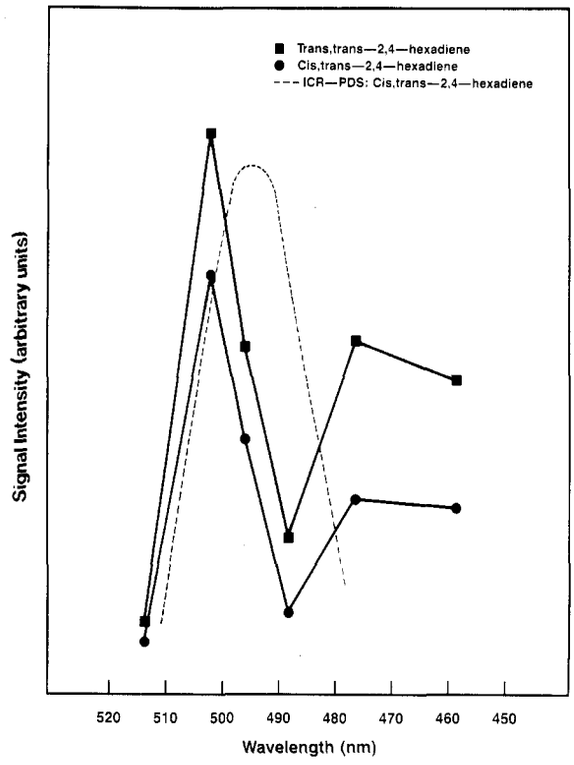

Figure 3. Photofragment ion spectra for *cis,trans*-2,4-hexadiene (●) and *trans,trans*-2,4-hexadiene (■). The ICR-PDS spectrum (dashed line) of *trans,trans*-2,4-hexadiene is included for comparison.

of the ion in the photon beam, we have corrected the branching ratios using a normalization constant of $(m_1/m_2)^{-1/2}$. The corrected photofragment ion abundances were summed and the photofragment ion branching ratios calculated as a percentage of the total photofragment ion signal.

The relative kinetic energies of the photofragment ions were measured for loss of H and CH_3 for the $C_5H_8^+$ and $C_6H_{10}^+$ isomers in the wavelength range 514.5–476 nm. Owing to the low relative abundances of the other photofragment ions (reactions 2, 4, 5, and 8), these measurements were not made for these reaction channels. The data for the photofragment ion relative kinetic energies can be used to calculate the amount of internal energy of the precursor ion partitioned as energy of translation, i.e., the kinetic energy release (T) value. The T values are calculated from the full width at half maximum (fwhm) of the photofragment ion signals and corrected for the main beam contribution to the peak width using eq 1 (*15*).

$$T = \frac{m_2^2 V(\Delta V_{m^*} - \Delta V)^2}{16 m_1 m_3 V^2} \quad (1)$$

In eq 1 V is the normal accelerating voltage, ΔV_{m^*} is the fwhm of the photofragment ion peak, ΔV is the fwhm of the main beam peak, and m_1, m_2, and m_3 are the masses of the precursor ion, photofragment ion, and product neutral, respectively. For the Gaussian peak shape the T values obtained by eq 1 correspond to the most probable product relative kinetic energy (*15*). The T values for the unimolecular and photodissociation reactions for the $C_5H_8^+$ ions are displayed graphically in Figure 4. The *cis*-$C_5H_8^+$ ions show typical behavior for T values as a function of photon wavelength (internal energy). The T value for the unimolecular loss of H being 170 meV, while the T value for the photoinduced reaction increases to a constant value of ca. 220 meV. The T value for loss of CH_3 shows similar behavior, i.e., 65 meV (unimolecular) and 70–88 meV (photoinduced). This contrasts with the behavior for the *trans*-$C_5H_8^+$ ions where a substantial wavelength dependence is observed for both loss of H and CH_3. In fact, for the *trans*-$C_5H_8^+$ iosmer there appears to be two distinct T value ranges. For example, at low-photon energies (514.5–502 nm or 2.41–2.49 eV), the T value for H loss increases approximately linearly (80–100 meV), whereas at higher photon energies (488–458 nm or 2.54–2.71 eV) the T value levels off to a constant value of 100 meV. The wavelength (or energy) dependent T value associated with loss of CH_3 appears to be made up of two overlapping functions. The low-energy region is characterized by a linear increase from 42 to 55 meV, while the high-energy region is characterized by an increase of different slope (120–224 meV).

The unimolecular and photoinduced T values for loss of H and CH_3 from *cis,trans*- and *trans,trans*-$C_6H_{10}^+$ ions are shown in Figure 5. Again, the photoinduced T values are very different for the two isomers. The unimolecular loss of H from *cis,trans*-$C_6H_{10}^+$ is accompanied by a T value of 85 meV, and the photodissociation reaction gives a T value between 110 and 155 meV. Over the photon wavelength range examined the T value increases in an approximately linear manner. For the CH_3 loss reaction channel, the unimolecular T value is 25 meV and the photoinduced T value is relatively constant (60 meV) over the wavelength range studied. The T values for loss of H from the *trans,trans*-$C_6H_{10}^+$ are quite similar to those of the *cis,trans*-$C_6H_{10}^+$ ions. That is, the unimolecular T value is 30 meV and the photoinduced T value is 50 meV and reasonably independent of photon wavelength. This behavior contrasts markedly with the behavior for CH_3 loss from the *trans,trans*-$C_6H_{10}^+$ ions. For example, the unimolecular T value is 150 meV, while the photoinduced T value decreases from 190 meV to 115 meV as the photon energy is increased from 514.5 nm (2.41 eV) to 458 nm (2.71 eV).

DISCUSSION

The ICR-PDS of dienes has been observed to exhibit characteristic spectra with well-defined structure in the 400–500 nm range (*16*). The laser–ion beam photodissociation spectra of the 1,3-pentadiene $C_5H_8^+$ ions (mixed isomers) has been previously reported and shows a broad absorption band in the 450–515 nm range with no real distinct maximum (*17*). It is not clear, however, that the reported spectra have been corrected for changes in the photon flux. The laser–ion beam photodissociation spectra reported here for the *cis*- and

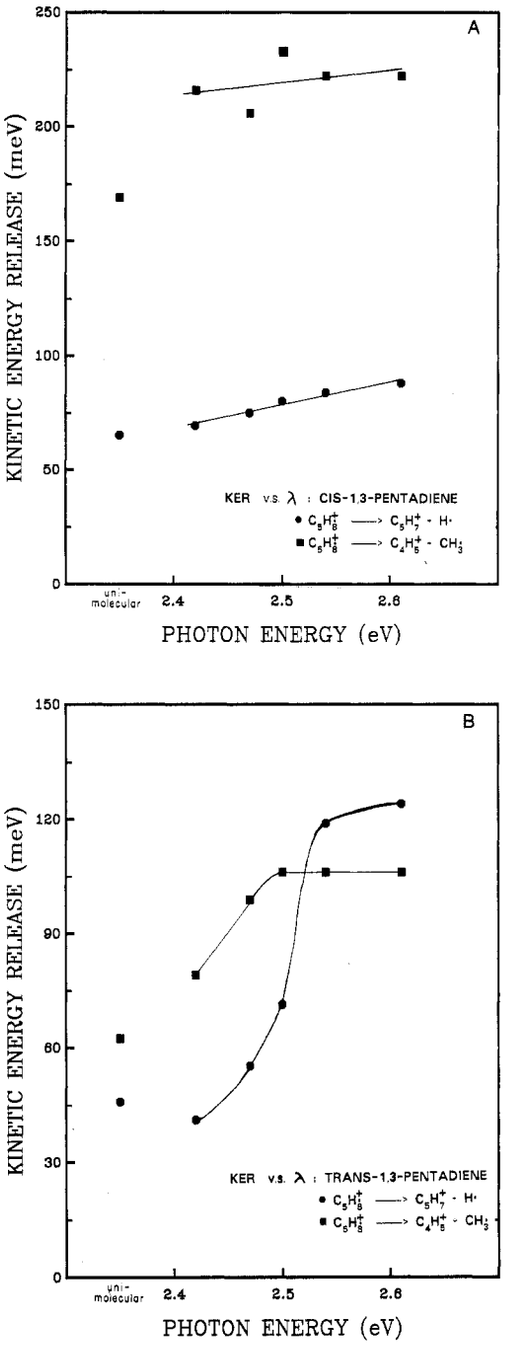

Figure 4. Kinetic energy release vs. photon energy for loss of H (■) and CH_3 (●) from (A) *cis*-1,3-pentadiene and (B) *trans*-1,3-pentadiene.

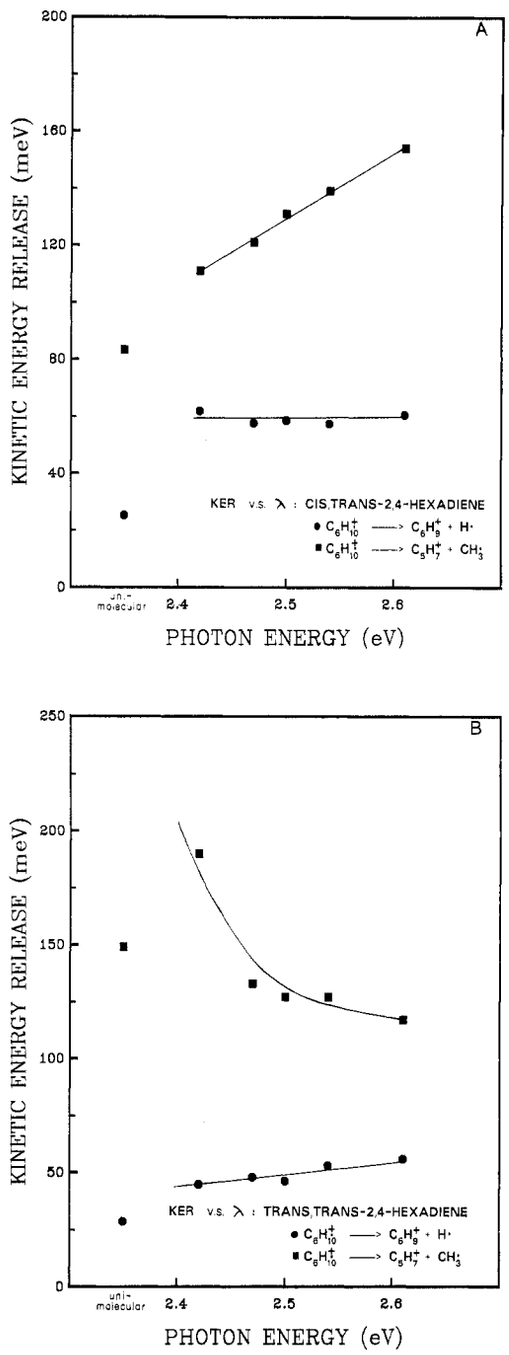

Figure 5. Kinetic energy release vs. photon energy for loss of H (■) and CH_3 (●) from (A) *cis,trans*-2,4-hexadiene and (B) *trans,trans*-2,4-hexadiene.

trans-$C_5H_8^+$ ions are indistinguishable, exhibiting maxima at 502 and 476 nm. The 502-nm maximum is in good agreement with the photoelectron spectroscopy (PES) data which predict photodissociation maxima at 511 nm and 499 nm for *cis*- and *trans*-$C_5H_8^+$ ions, respectively (*18*). However, because the photodissociation spectra are so similar, structural assignment for the two isomers cannot be made using only the spectral data.

The ICR-PDS spectra of the three geometric isomers of 2,4-hexadiene have also been reported (*3*). The spectra exhibit broad absorption bands (25 nm fwhm) with maxima at approximately 502 nm, 493 nm, and 488 nm for *cis,cis*-, *trans,trans*-, and *cis,trans*-$C_6H_{10}^+$ ions, respectively. The laser–ion beam photodissociation spectra of the *cis,trans*- and *trans,trans*-$C_6H_{10}^+$ ions agree qualitatively with the ICR-PDS results with an observed maxima at 502 nm (15 nm fwhm) for both isomers. This qualitative agreement is reasonable since the ICR experiment was performed with a tunable dye laser and our studies were performed with an argon ion laser yielding line spectra in which the data points have been arbitrarily connected. In addition, the maximum at 502 nm agrees with the PES which predicts photodissociation maxima at 501 nm and 507 nm for *trans,trans*- and *cis,trans*-$C_6H_{10}^+$ (*18*).

The ICR-PDS has not been reported for the wavelength range below 484 nm; therefore no comparison can be made with the laser–ion beam photodissociation maxima observed at 476 nm. Although Dunbar was able to differentiate the three geometric isomers of 2,4-hexadiene radical cations by inspection of the ICR-PDS spectra, the spectra reported here do not exhibit distinguishable shifts in the photofragment maxima. The lack of distinguishable spectral data are probably due to an insufficient number of laser wavelengths in the absorption region to allow accurate assignment of the photodissociation maxima. Therefore, as is the case with the

1,3-pentadienes, structural assignment of the geometric isomers cannot be made based on the photofragment spectral data alone.

The photofragment ion branching ratios are, within the experimental error, identical for the two 1,3-pentadiene ions in the wavelength range 514.5–476 nm. The change in the branching ratios at 458 nm is quite possibly due to internal energy effects (*19*). Internal energy effects will be strongest in cases where the energy of the photoexcited ion lies near the threshold for dissociation. The branching ratio data suggest that the threshold for CH_3 loss from $C_5H_8^+$ ions is between 2.61 eV (476 nm) and 2.71 eV (458 nm) above the energy of the ground state ion. The appearance energy for $C_4H_5^+$ ions from *trans*-$C_5H_8^+$ has been reported as 12.57 eV (3.2 eV above the ground state) (*14*). At photon energies less than 2.71 eV, the branching ratios are reasonably constant with preferential loss of H; i.e., the lowest energy reaction channel is preferred; the appearance energy for H loss is 1.6 eV (*14*)). At 2.71 eV a larger fraction of the $C_5H_8^+$ ions has sufficient energy to dissociate via the higher energy CH_3 loss reaction channel. The branching ratios at 458 nm are somewhat different for the *cis*- and *trans*-$C_5H_8^+$ ions with the trans isomer favoring CH_3 loss (23% vs. 17%). This difference may be due to a small difference in the appearance energies for loss of CH_3 from the two isomers. Regardless, this difference is small and structural assignment of the two isomers based solely on this difference in the product ion branching ratios would not be acceptable.

The branching ratios for the potodissociation of the *cis,trans*- and *trans,trans*-$C_6H_{10}^+$ ions are also indistinguishable over the entire wavelength range studied. It is interesting to note that the trans,trans isomer favors dissociation by CH_3 loss as compared to the cis,trans isomer. Again, this may be due to a small difference in the energetics for dissociation.

Although the laser–ion beam photofragment ion spectra and branching ratio data are not sufficiently different to allow unequivocal structural assignment for either the pentadienes or the hexadienes, the wavelength-dependent photofragment kinetic energy release (T) values are unique for the reactant ion. The T data for the *cis*-$C_5H_8^+$ ion shows a near linear increase with photon energy for both H and CH_3 loss. Based on the assumption that the experimentally measured T value arises from both reverse-activation energy and excess energy, the T value, assuming statistical behavior, should increase with photon energy (*20*). That is, as the energy of the dissociating ion increases, the amount of excess energy partitioned as energy of translation also increases. The kinetic energy release behavior for the *trans*-$C_5H_8^+$ ion is not adequately explained by such a simple model. It is apparent that for both H and CH_3 loss, a threshold is reached at approximately 500 nm (2.48 eV) that is observable in the T value. This threshold could correspond to (1) isomerization of the reactant ion following photoexcitation but preceding dissociation or (2) formation of a second product ion structure. Isomerization of the $C_5H_7^+$ and $C_4H_5^+$ product ions cannot be ruled out, but it seems unlikely that the threshold for isomerization of two different product ions would occur at the same energy. It is possible to rule out isomerization of the *trans*-$C_5H_8^+$ ion to the *cis*-$C_5H_8^+$ ion since the T values at energies greater than 500 nm are still very different for the two isomers. The most plausible explanation for the wavelength-dependent T values is that at energies greater than 500 nm, isomerization of the trans isomer precedes dissociation and that this second structure is characterized by a different wavelength dependence for T.

The *cis,trans*- and *trans,trans*-$C_6H_{10}^+$ ions can also be differentiated by the different wavelength-dependent T values. For the cis,trans isomer the observed behavior is typical and examples of both the near-linear increase, as observed for H loss, and the constant T value, as observed for CH_3 loss, have been reported (*12*, *13*, *21*). The trans,trans isomer shows a modest difference in the CH_3 loss reaction channel, i.e., a small increase in T as the photon energy is increased. However, the H loss reaction channel differs significantly for the two isomers. In fact, the T value for H loss from *trans,trans*-$C_6H_{10}^+$ ion decreases significantly as the photon energy is increased. Although this type of behavior has been reported, it has not been completely explained.

For both *trans*-$C_5H_8^+$ and *trans,trans*-$C_6H_{10}^+$ ions we propose that structural isomerization occurring prior to dissociation accounts for the unusual photodissociation T vs. photon wavelength behavior. Structural isomerization of $C_5H_8^+$ ions, e.g., 1-methylcyclobutene, 3-methylcyclobutene, and 2-methyl-1,3-butadiene, was the subject of a recent paper by Dass, Sack, and Gross (*22*). These authors conclude that the 1- and 3-methylcyclobutene radical cations undergo a facile electrocyclic ring-opening reaction to give 1,3-pentadiene ion. Activation energies for the ring-opening reaction are reported to be 14 kcal mol^{-1} and 4 kcal mol^{-1} for the 1- and 3-methylcyclobutene ions, respectively. The general question of electrocyclic reactions of cyclobutene radical cations has been the subject of several experimental studies (*23–25*). Owing to the problems associated with differentiation of structural isomers, the occurrence of such reactions is rather difficult to probe. On the basis of the results of the present work, it may be possible to probe these questions directly using laser–ion beam photodissociation.

For example, based on Woodward–Hoffman rules of conservation of orbital symmetry (*26*), isomerization of *trans,trans*-2,4-hexadiene and *trans*-3,4-dimethylcyclobutene should be thermally "allowed". If we assume that these considerations hold for open-shell systems, a similar isomerization should be feasible for the same $C_6H_{10}^+$ radical cations. The general conclusions from the work of Gross is that cyclobutene ions with low internal energies (stable, nondissociating ions) undergo a low activation energy electrocyclic ring opening (*22*). The results from the laser–ion beam photodissociation studies are interpreted here as evidence that highly activated linear diene radical cations undergo a similar isomerization reaction. Quite possibly, the driving force for the cyclization reaction is the stability of the product ion. One could simply argue that the activated $C_6H_{10}^+$ ions dissociate by loss of H to give the methylcyclopentenium ($C_6H_9^+$) ions as suggested by Holmes (*27*). However, this argument would predict that the *cis,trans*- and *trans,trans*-$C_6H_{10}^+$ ions would behave similarly. An argument based on the Woodward–Hoffman rules, however, would explain the apparent isomerization of the trans,trans isomer to *trans*-3,4-dimethylcyclobutene ions.

The present interpretation of the photodissociation data is consistent with Bowers' kinetic model for the dissociation of 1,3-butadiene $C_4H_6^+$ (*28*). That is, ions ($C_4H_6^+$, $C_5H_8^+$, or $C_6H_{10}^+$) with energies near the dissociation threshold isomerize prior to dissociation, whereas at higher internal energies dissociation without isomerization is favored. The threshold for isomerization vs. "direct" dissociation corresponds to the changeover in the measured T values. Thus, at low photon energies the photoexcited ion isomerizes to a cyclobutene structure prior to dissociation, and the measured T value is that for a decomposing dimethylcyclobutene $C_6H_{10}^+$ ion. At higher photon energies, the dissociation rate exceeds the isomerization rate, and the decomposing ion has a linear diene structure. More detailed experiments, e.g., isotopic labeling, kinetic isotope effects, etc., to test further this hypothesis are under way.

Registry No. *cis*-1,3-Pentadiene, 1574-41-0; *trans*-1,3-pentadiene, 2004-70-8; *cis,trans*-2,4-hexadiene, 5194-50-3; *trans,trans*-2,4-hexadiene, 5194-51-4.

LITERATURE CITED

(1) Orth, R. G.; Dunbar, R. C. *J. Am. Chem. Soc.* **1978**, *100*, 5949.
(2) Orth, R. G.; Dunbar, R. C. *J. Am. Chem. Soc.* **1982**, *104*, 5617.
(3) Benz, R. C.; Dunbar, R. C.; Claspy, P. C. *J. Am. Chem. Soc.* **1981**, *103*, 1799.
(4) Dunbar, R. C.; Teng, H. H. *J. Am. Chem. Soc.* **1978**, *100*, 2279.
(5) Kramer, J. M.; Dunbar, R. C. *J. Chem. Phys.* **1973**, *59*, 3092.
(6) van Tilborg, M. W. E.; van Thijl, J.; van der Hart, W. J. *Org. Mass Spectrom.* **1984**, *19*, 149.
(7) van Zalen, P. N. T.; van der Hart, W. J. *Chem. Phys.* **1981**, *61*, 335.
(8) Gooden, R.; Brauman, J. I. *J. Am. Chem. Soc.* **1982**, *104*, 1483.
(9) Dunbar, R. C. In "Molecular Ions: Spectroscopy, Structure, and Chemistry", Miller, T. A., Bondybey, V. E., Eds.; North Holland Publishing Co.: Amsterdam, 1983.
(10) Mukhtar, E. S.; Griffiths, I. W.; March, R. E.; Harris, F. M.; Beynon, J. H. *Int. J. Mass Spectrom. Ion Phys.* **1981**, *41*, 61.
(11) Griffiths, I. W.; E. S. Mukhtar; Harris, F. M.; Beynon, J. H. *Int. J. Mass Spectrom. Ion Phys.* **1981**, *38*, 333.
(12) Mukhtar, E. S.; Griffiths, I. W.; Harris, F. M.; Beynon, J. H. *Int. J. Mass Spectrom. Ion Phys.* **1982**, *42*, 77.
(13) Mukhtar, E. S.; Griffiths, I. W.; Harris, F. M.; Beynon, J. H. *Org. Mass Spectrom.* **1981**, *16*, 51.
(14) Rosenstock, H. M.; Draxl, K.; Steiner, B. W.; Heron, J. T. *J. Phys. Chem. Ref. Data* **1977**, *6*, Suppl. 1.
(15) Cooks, R. G.; Beynon, J. H.; Caprioli, R. M.; Lester, R. G. "Metastable Ions"; Elsevier: New York, 1973.
(16) Dunbar, R. C. *Anal. Chem.* **1976**, *48*, 723.
(17) Weger, E.; Wagner-Redeker, W.; Levsen, K. *Int. J. Mass Spectrom. Ion Phys.* **1983**, *47*, 77.
(18) Bieri, G.; Burger, F.; Heilbronner, E.; Maier, J. P. *Helv. Chim. Acta* **1977**, *60*, 145.
(19) Kalliler, R. E.; Russell, D. H. *Org. Mass Spectrom.*, in press.
(20) Lifshitz, C.; Gefen, S.; Arakawa, R. *J. Phys. Chem.* **1984**, *88*, 4242.
(21) Krailler, R. E.; Russell, D. H.; Jarrold, M. F.; Bowers, M. T. *J. Am. Chem. Soc.*, in press.
(22) Dass, C.; Sack, T. M.; Gross, M. L. *J. Am. Chem. Soc.* **1984**, *106*, 5780.
(23) Hoffman, M. K.; Bursey, M. M.; Winter, R. E. K. *J. Am. Chem. Soc.* **1970**, *92*, 727.
(24) Gross, M. L.; Russell, D. H. *J. Am. Chem. Soc.* **1979**, *101*, 2082.
(25) Dass, C.; Gross, M. L. *J. Am. Chem. Soc.* **1983**, *105*, 5724.
(26) Woodward, R. B.; Hoffman, R. *J. Am. Chem. Soc.* **1965**, *87*, 395.
(27) Wolkoff, P.; Holmes, J. L. *Can. J. Chem.* **1979**, *57*, 348.
(28) Jarrold, M. F.; Bass, L. M.; Kemper, P. R.; van Koppen, P. A. M.; Bowers, M. T. *J. Am. Chem. Soc.* **1983**, *78*, 3756.

RECEIVED for review December 13, 1984. Accepted February 15, 1985. This work was supported by the U.S. Department of Energy, Office of Basic Energy Sciences (DE-AS05-82ER13023), and the Robert A. Welch Foundation. Some of the equipment used for this work was purchased from funds provided by the Texas A&M University Center for Energy and Mineral Resources.

Beam Geometry Optimization in Dual-Beam Thermal Lensing Spectrometry

Thierry Berthoud,* Nathalie Delorme, and Patrick Mauchien

DCAEA/SEA/SEACC, Centre d'Etudes Nucléaires, 92260 Fontenay-aux-Roses, France

This paper describes the first systematic study of the influence of beam geometric positions in dual-beam thermal lensing spectrometry. Intensity and sign of thermal lens signals are studied varying both beam waist and measurement cell locations. A theoretical model, involving beam sizes in the cell, is proposed to explain the experimental data. These results indicate that differential dual-beam thermal lensing should be possible with either pulsed or continuous excitation. Usually limited by nonspecific solvent absorption, very low level concentration determination can therefore be considered.

Several recent studies of weak absorption measurements have been realized by using thermal lensing spectrometry and optoacoustic spectroscopy. These techniques have been demonstrated to be very powerful tools for low-level determination of nonfluorescent molecular species in solution. Thermal lensing spectrometry reaches limits of detection 100–1000 times lower than classical absorption spectrophotometry LOD (*1–7*).

The first experimental thermal lensing studies have been made with single-beam arrangements where the beam both creates and probes the thermal lens in the sample. Afterward, dual-beam configurations have been employed where another beam (usually He–Ne) probes the thermal lens formed in the sample by the excitation beam.

In dual-beam schemes, most investigators have used a single lens to focus both excitation and probe laser beams. The sensitivity of the thermal lens signal has been investigated in regard to the locations of the pump and probe beam waists in the sample cell. Assuming that the two beam sizes are nearly the same in the sample, when the single- and dual-beam setups are compared, the signal magnitudes only depend on their respective wavelengths (*8–13*).

Although Fang and Swofford have suggested that mismatched waists of the two beams give enhanced sensitivity, no systematic study has been published about geometry of dual-beam arrangements (*16*). This work proposes a theoretical interpretation of experiments relating the probe beam waist to its position toward the excitation beam waist.

Such experiments and their explanations are determinant for further investigations for an eventual extension of the differential thermal lensing technique, studied for single-beam measurements by Dovichi and Harris (*11*), to dual-beam measurements with either continuous or pulsed excitation.

EXPERIMENTAL SECTION

The experimental setup is schematically depicted in Figure 1. The excitation laser beam is produced by a tunable dye laser (Spectra-Physics Model 380 C) pumped by a 5-W argon ion laser (Spectra-Physics Model 165) working in the light control mode. Experiments are performed with a neodymium solution of 5×10^{-4} mol/L in distilled water. The dye laser is tuned to the maximum absorption wavelength of neodymium at 575 nm and adjusted to a power of 500 mW.

The dye laser beam, chopped at a frequency of 1 Hz, is focused by a 20-cm focal length lens. The probe beam is focused, prior to the beam splitter, with a 33-cm focal length lens, mobile on a 30-cm path. After passing through the absorbing solution in a quartz cell, the excitation beam at 575 nm is filtered out and the He–Ne beam is directed through a pinhole of 1-mm diameter after an optical path of 2.5 m. The photodiode current is amplified with a current amplifier (Keithley Model 427) and sent to a digital

0003-2700/85/0357-1216$01.50/0